High-energy magnetic excitations and anomalous spin-wave damping in $FeGe_2$

2000 J. Phys.: Condens. Matter 12 8487

(http://iopscience.iop.org/0953-8984/12/39/311)

J. Phys.: Condens. Matter **12** (2000) 8487–8493. Printed in the UK PII: S0953-8984(00)15871-0

High-energy magnetic excitations and anomalous spin-wave damping in $FeGe_2$

C P Adams†¶, T E Mason†+, E Fawcett†*, A Z Menshikov‡*, C D Frost§, J B Forsyth§, T G Perring§ and T M Holden‖#

† Department of Physics, University of Toronto, Toronto, ON, Canada M5S 1A7
‡ Institute for Metal Physics, Ekaterinburg, Russian Federation
§ ISIS Facility, Rutherford-Appleton Laboratory, Chilton, Didcot OX11 0QX, UK
‖ National Research Council, Chalk River, ON, Canada K0J 1J0

E-mail: carl.adams@nist.gov.

Received 27 July 2000

Abstract. Inelastic neutron scattering has been used to measure the high-energy, low-temperature magnetic excitations of the itinerant antiferromagnet $FeGe_2$. The spin-wave excitations follow a Heisenberg dispersion with exchange constant along the c-axis $SJ_{FM} = 68 \pm 1$ meV an order of magnitude higher than the basal-plane antiferromagnetic constant $SJ_{AFM} = -4.4 \pm 0.6$ meV. The c-axis spin waves are highly damped, even at temperatures small compared to SJ_{FM}. The damping is roughly quadratic in energy (as in the hydrodynamic model) up to ∼250 meV, beyond which a continuum of excitations emerges.

1. Introduction

Over the last 10 years there has been growing evidence that a nearby spin-density-wave (SDW) instability is responsible for the anomalous normal-state transport properties of the high-T_c oxides [1] and possibly for the superconductivity itself [2–5]. Similar instabilities precede the SDW transitions in certain other Mott–Hubbard systems [6], such as $V_{2-y}O_3$ [7]. In both cases, strong electron–electron correlations exist and lead to a breakdown of conventional band theory and, as in the high-T_c cuprates, a metal–insulator transition. Despite some obvious differences these novel SDW systems have much in common with non-correlated, fully metallic, SDW systems, of which chromium [8] is the prototypical example. Notably in all SDW systems the periodic modulation of the conduction-electron spin density [9] develops as a result of Fermi surface nesting, i.e., electron exchange between two parallel pieces of Fermi surface [10]. In the light of this commonality the recent interest in the high-T_c oxides has led to renewed studies of non-correlated SDW systems, where conventional band theory should be able to answer outstanding questions regarding transport and magnetic properties.

One intriguing feature, common to both correlated and non-correlated SDW systems, is a complex spectrum of magnetic excitations in both ordered and non-ordered phases;

¶ Present address: NIST Center for Neutron Research, National Institute of Standards and Technology, Gaithersburg, MD 20899-8562, USA.
+ Present address: Spallation Neutron Source, 701 Scarboro Road, Oak Ridge National Laboratory, Oak Ridge, TN 37830, USA.
* Deceased.
# Retired.

0953-8984/00/398487+07$30.00

conventional oscillatory, propagating spin waves do not exist in these materials [7, 8, 11, 12]. This has greatly hindered a complete description of SDW systems since it is the spin-wave dispersion that yields values for the microscopic interaction strengths. From this viewpoint $FeGe_2$, the non-correlated SDW system that is the subject of this study, is an important exception, since the first inelastic neutron scattering measurements showed that its low-temperature magnetic excitations *are* propagating spin waves or magnons [13, 14]. A simple Heisenberg model successfully describes the low-energy magnetic dispersion. However, there appears to be an intrinsic damping of the spin waves even at low temperatures. Damping of this magnitude is impossible in a purely localized system where magnon–magnon and magnon–phonon scattering processes dominate, but in metallic systems, such as $FeGe_2$, scattering can simply arise from the itinerant electrons even at low T. This dual behaviour (spin-wave dispersion of local moments, significant damping from itinerant electrons) is also found in the ferromagnetic (FM) metals iron [15] and nickel [16] and $La_{0.85}Sr_{0.15}MnO_3$ [17], a FM transition metal oxide near the Mott transition.

A further novel feature of $FeGe_2$ is that the dispersion is so anisotropic that it is well described as quasi-one-dimensional (quasi-1D), unique among metallic magnetic systems [14]. While the entire a-axis magnon dispersion was measured using thermal neutron scattering at the Chalk River reactor, the much larger energy scale associated with the c-axis magnons prevented the observation of resolved spin-wave modes in constant-Q scans. A quantitative determination of the damping (seen as the intrinsic linewidth) and the high-Q dispersion was not possible. This prompted a continuation of these measurements up to higher energies at the ISIS spallation source.

$FeGe_2$ has a body-centred tetragonal crystal structure, as in $CuAl_2$, with space group $I4/mcm$ and two zero-field magnetic phase transitions [18, 19]. One is a second-order Néel transition from a paramagnetic phase to an incommensurate (IC) SDW state at $T_N = 289$ K and the other at $T_{C-IC} = 263$ K is a typical first-order transition from an IC to a commensurate phase [19]. The ordering wavevector of the commensurate phase, $(2\pi/a)(1, 0, 0)$, changes to $(2\pi/a)(1 + \delta, 0, 0)$ in the IC phase where δ varies from 0 to $\sim$0.05. Nearest-neighbour (NN) iron atoms are 2.478 Å apart along the c-axis and their magnetic moments have FM alignment in both phases. The next-NN iron atoms are separated by 4.178 Å along the [110] direction with antiferromagnetic (AFM) alignment of the moments below T_{C-IC}. The higher-temperature IC phase appears as a long-wavelength modulation of this structure in the basal plane. AFM IC structures in metals are a strong indication of an interaction that is mediated by the conduction electrons (indirect exchange). Superexchange through the germanium ions probably also plays a role in the net AFM basal-plane interaction. In contrast, the NN spacing along the c-axis is so close to that of elemental iron (2.50 Å) that the primary magnetic interaction in this direction is probably a direct FM interaction.

2. Experimental results and discussion

To measure the high-energy magnetic excitations and the damping of spin waves in $FeGe_2$, a new single crystal sample was prepared. It is roughly semi-cylindrical, 15 mm in radius and 40 mm in length, with a mass of 270 g. The measurements were performed at 11 K in the low-T AFM phase (effectively at $T = 0$ compared to T_N) using HET, a direct-geometry chopper spectrometer at the ISIS spallation source. The sample was oriented with [010] vertical so the horizontal banks of detectors were sensitive to momentum transfers $\boldsymbol{Q}$ with $(h0l)$ components, designated by Q_a and Q_c. Since HET is a time-of-flight instrument, energy transfer E is coupled to $\boldsymbol{Q}$ in a way that in general prevents extraction of constant-E and constant-Q scans (conventionally employed when using a triple-axis spectrometer). Despite this complication,

a substantial part of the magnetic dispersion can often be measured at one time provided that a suitable orientation of the sample is chosen.

An example of an HET scan is shown in figure 1. The curved surface in $(\boldsymbol{Q}, E)$ space scanned by the instrument is projected onto the (Q_a, Q_c) plane. The contours of constant-E reflect this curvature and approach the incident energy $E_i = 120$ meV at the apex. Absolute scattering intensity, resulting from vanadium normalization, is indicated by spectral colour. In terms of actual neutron counts, 1 mb meV^{-1} sr^{-1} is equal to 20 counts over a 12-hour scan. No correction was made for sample shape or absorption, which could lead to an error of 15% in the absolute cross-section values. Several features are evident in figure 1: incoherent elastic scattering along the $E = 0$ contour, complicated phonon and magnon scattering for $E < 40$ meV, and beyond that 'rabbit ear' structures extending to high E which emanate from the FM zone centres at $Q_c = 0$ and 2 c^*. These 'rabbit ears' are the c-axis magnons. Their dispersion is steep with only a slight change in Q_c from $E = 40$ meV to $E = 110$ meV. The dispersion is also quasi-1D; the range of Q_a spans several zones without any obvious periodic 'ring' or 'wave' structures.

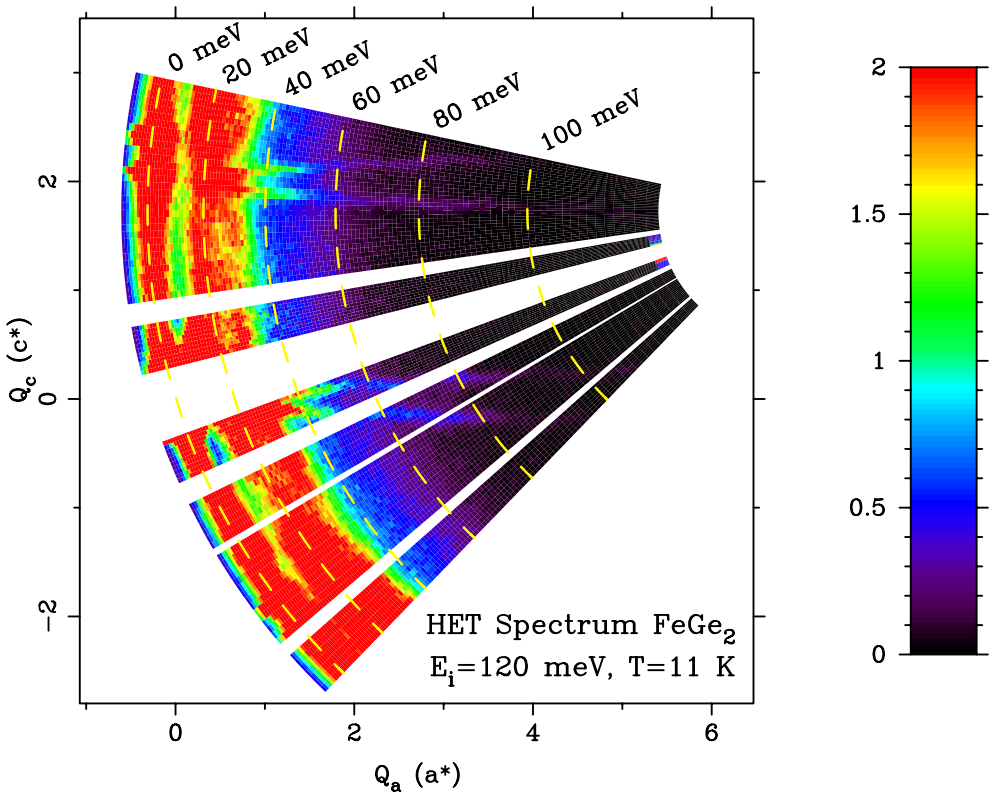

Figure 1. An HET scan showing the scattered neutron intensity projected onto the (Q_a, Q_c) plane. with constant-E contours in yellow. Intensity is given by the spectral colour scale in units of mb meV^{-1} sr^{-1}. The 'rabbit ear' features emanating from $Q_c = 0$ and 2 c^* are the c-axis magnons.

Reduction to 1D dispersion greatly simplifies the data interpretation. Q_a is discarded and the scattered intensity is plotted in the (Q_c, E) plane, allowing the extraction of meaningful constant-E and constant-Q scans as cuts through the data of figure 1. Several of these cuts

for various values of E_i are shown in figures 2(a) and 2(b) and resemble the more familiar constant-E and constant-Q triple-axis scans. Peaks are resolved to high energies (>200 meV) in both types of cut. The dispersion, which is quite steep in comparison to the Q_c-resolution, is measured with a resolution corrected fit to the peaks in constant-E cuts as shown in figure 2(a). The constant-Q_c cuts show damped magnons with a significant linewidth that increases with energy. Along the a-axis, similar spin-wave behaviour and damping have been observed with triple-axis measurements [13] but the zone boundary energy is only 30 meV, much less than the c-axis spin-wave energies in figures 2(a) and 2(b).

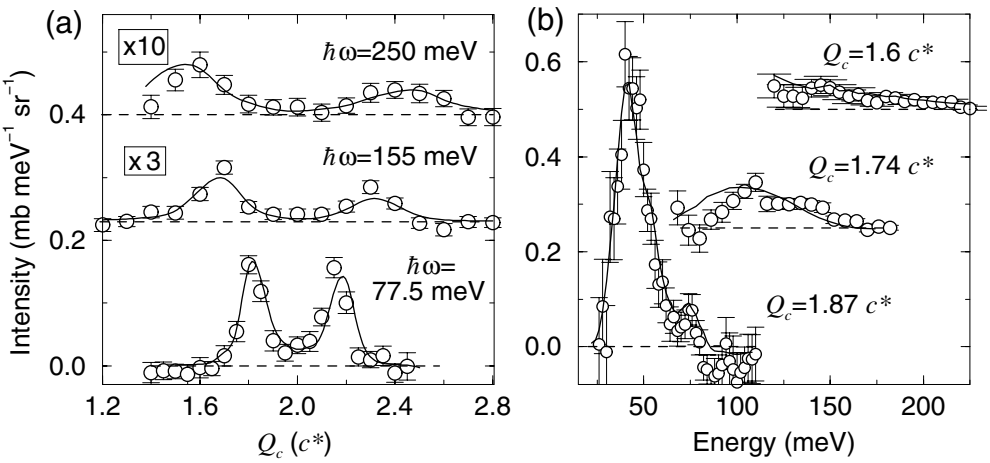

Figure 2. (a) Constant-E and (b) constant-Q_c cuts showing the c-axis magnons. Cuts are taken from data reduced to the (Q_c, E) plane and have been offset vertically (the thick dashed lines represent zero intensity above the background). Two sets have been rescaled as indicated. The data in (b) have had the background removed by subtraction of a nearby non-magnetic cut. The solid lines are the resolution-corrected scattering cross-sections (described in more detail in a later section).

The c-axis spin-wave dispersion, as measured by Gaussian fits to constant-E cuts, is shown in figure 3.

The 3D classical, NN Heisenberg model has a Hamiltonian of the form

$$H = -\sum J_{ij} \boldsymbol{S}_i \cdot \boldsymbol{S}_j.$$

Combining this with the known low-T AFM structure of $FeGe_2$ gives the spin-wave dispersion [20]:

$$\hbar\omega_Q = 4S(\{J_{FM}[1-\cos(\pi l)] - 2J_{AFM}[1-\cos(\pi h)\cos(\pi k)]\} \times \{J_{FM}[1-\cos(\pi l)] - 2J_{AFM}[1+\cos(\pi h)\cos(\pi k)]\})^{1/2} \quad (1)$$

where the spin-wave energy is $\hbar\omega_Q$, S is the on-site spin, J_{FM} is the c-axis exchange constant, J_{AFM} is the [110] exchange constant, and h, k, and l express $\boldsymbol{Q}$ in terms of reciprocal-lattice coordinates. Triple-axis measurements [13] have shown a gapless (<2 meV) dispersion and we analysed our results in this manner. This implies that the single-ion anisotropy is negligible, another result in conflict with a large local iron moment. Previously we used a planar 1D model [21] to describe the c-axis dispersion [14]. This greatly simplified the data analysis since the magnon energies were independent of Q_a and the data in figure 3 of reference [14] are in fact over several magnetic zones. This had the effect of making the low-Q_c quadratic dispersion appear quite linear and gave a large out-of-plane anisotropy (but does not lead to a

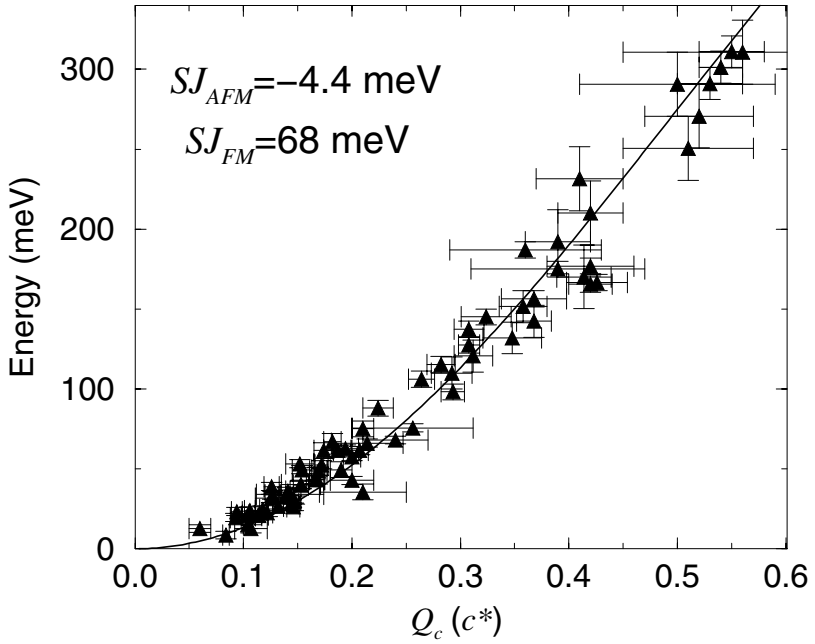

Figure 3. The c-axis magnon dispersion and the prediction of a NN Heisenberg model. The data have been corrected for the Q_a-energy contribution. Excitations beyond the plotted E-range are highly damped and not well defined.

gap in the 1D planar model). However, using equation (1) with $SJ_{AFM} = -4.4$ meV (from the data of [13]) significantly improves the fit to the low-energy dispersion and the overall scattered intensity (see the next section). The 3D behaviour can be seen in figure 2(b) where the variation in Q_a along a 'constant-Q' cut leads to peaks at 45 meV and at 75 meV for $Q_c = 1.87\,c^*$; an effect that is correctly predicted by the simulation. The small Q_a-dependent energy contribution arising from equation (1) has been subtracted from the data in figure 3 to leave only the Q_c-dependence. The system becomes more 1D at higher energies as this correction decreases in comparison to $\hbar\omega_Q$. The fit shown in figure 3 has $SJ_{FM} = 68 \pm 1$ meV, roughly a factor of 15 larger in strength than SJ_{AFM}, a uniquely large anisotropy among 3D metals.

Although the Gaussian fits give the dispersion of well defined magnons, they provide no clear information about the damping since the intrinsic linewidth remains convoluted with the experimental resolution. This linewidth is determined by using a simulation of the resolution and a full model for the scattering cross-section per iron atom [20]:

$$\frac{\mathrm{d}^2\sigma}{\mathrm{d}\Omega\,\mathrm{d}E'} \propto \frac{k_f}{k_i}|F(Q)|^2\left(\frac{J_{FM}[1-\cos(\pi l)]-2J_{AFM}[1-\cos(\pi h)\cos(\pi k)]}{J_{FM}[1-\cos(\pi l)]-2J_{AFM}[1+\cos(\pi h)\cos(\pi k)]}\right)^{1/2} \times\left[1-\exp\left(-\frac{E}{k_BT}\right)\right]^{-1}\left(\frac{4}{\pi}\frac{\hbar\omega_Q E\Gamma}{[E^2-(\hbar\omega_Q)^2]^2+4(E\Gamma)^2}\right). \tag{2}$$

k_i and k_f are the lengths of the incident and final neutron wavevectors. $F(Q)$ is a magnetic form factor appropriate for Fe^{3+} [22]. The next term, the dynamical structure factor, predicts that the intensity of pure FM spin waves is uniform throughout the magnetic Brillouin zone and AFM spin waves have a diverging intensity at magnetic zone centres and zero intensity at nuclear zone centres. The principle of detailed balance is satisfied by inclusion of the thermal

population of magnons. The final term is the appropriate susceptibility for a damped simple harmonic oscillator (DSHO) with linewidth Γ and free-mode energy $\hbar\omega_Q$. This cross-section correctly approaches δ-functions in the $\Gamma \ll \hbar\omega_Q$ limit.

The simulation, using equation (2) and the previously mentioned SJ-values, successfully describes the spin-wave intensity and dispersion through several magnetic Brillouin zones. Subsequent fixing of the proportionality in equation (2) gives the results for Γ shown in figure 4. This confirms that the peak broadening in figure 2 is due to increasing Γ rather than the coarsening resolution at higher E_i. The damping increases rapidly beyond $\hbar\omega_Q = 220$ meV, wiping out the well defined magnon peaks; uncertainties in peak position and linewidth increase accordingly. Such large values of Γ for $T \ll T_N$ are not expected on the basis of local models where magnon–magnon scattering dominates. Hence, this damping is anomalous and must be due to itinerant electrons, a conclusion previously reached in studies of several FM systems [15–17]. In fact, the itinerant effects eventually predominate over the local behaviour and the spin waves merge into a continuum of excitations ($\Gamma \sim E$). Calculation of Γ in itinerant systems often requires detailed knowledge of the electronic band structure [23] but in $FeGe_2$ the reduced dimensionality and the lack of electron correlations may simplify such a prediction, providing important insight into several classes of itinerant magnetic systems.

One result that appears to be preserved from a local-moment model is the quadratic variation of Γ with E predicted by the hydrodynamic model [24]. A range of appropriate quadratic parametrizations is shown in figure 4 with the best description being given for $\Gamma = 2.7 \times 10^{-3} E^2$ (meV units). The reciprocal of the prefactor is 370 ± 80 meV, comparable to $4SJ_{FM} = 272$ meV, half of the zone boundary energy. The hydrodynamic model includes SJ in a similar way but also includes a T-dependent term, $(T/T_N)^3$, which would eliminate low-T damping. This is clearly in disagreement with figure 4.

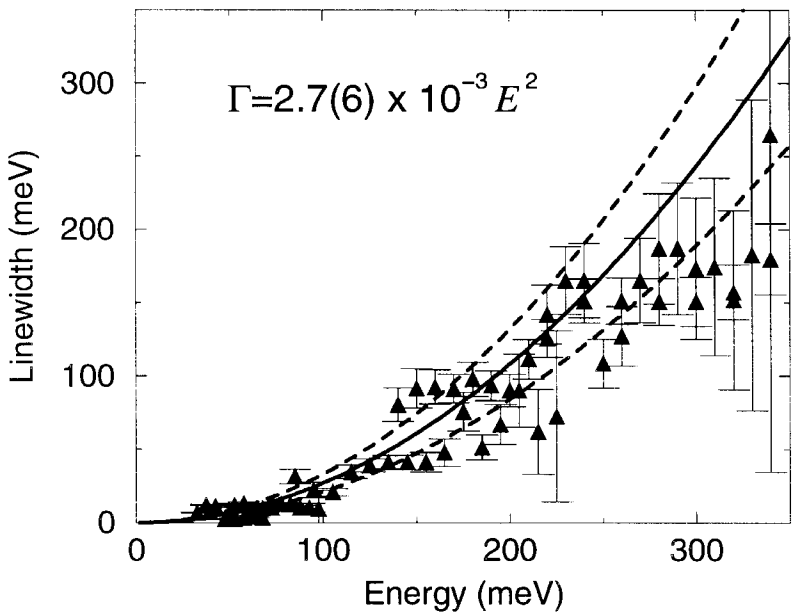

Figure 4. The magnon linewidth Γ versus E. The solid and dashed lines represent the function and the uncertainty given in the figure. Note the rapid increase of Γ beyond 220 meV and the gradual merging into a continuum of excitations.

The observation of well defined spin-wave modes in an itinerant system such as $FeGe_2$ is particularly noteworthy given the fact that this sort of response has not been seen in Cr, the prototypical SDW system. In Cr, complex behaviour at low frequencies is observed with a suggestion of spin-wave modes with a high velocity [8, 25]. However, measurements to higher frequencies carried out using the same time-of-flight techniques as are employed in the present study have failed to reveal resolved spin-wave modes such as those shown in figure 2. The behaviour of $FeGe_2$ is similar to that seen in itinerant FM materials where the magnon modes have non-zero damping, even in the low-T ground state. The reduced dimensionality of $FeGe_2$ may hasten a theoretical description of the transition from local to fully itinerant magnetism.

Acknowledgments

We wish to thank V G Guk from the Ural Technical University for growing the $FeGe_2$ single crystal and S M Hayden who provided the computer code for the resolution-corrected fits. Work at Toronto was supported by the Natural Sciences and Engineering Research Council of Canada and the Canadian Institute for Advanced Research. TEM acknowledges the support of the A P Sloan Foundation. AZM recognizes the support of the programme 'Neutron Study of Matter' and RFFI Grant No 98-02-16165.

References

[1] Takagi H, Ido T, Ishibashi S, Uota M, Uchida S and Tokura Y 1989 *Phys. Rev.* B **40** 2254
[2] Scalapino D J, Loh E Jr and Hirsch J E 1987 *Phys. Rev.* B **35** 6694
[3] Monthoux P, Balatsky A V and Pines D 1992 *Phys. Rev.* B **46** 14 803
[4] Levin K, Zha Y, Radtke R J, Si Q, Norman M R and Schüttler H-B 1994 *J. Supercond.* **7** 563
[5] Ruvalds J, Rieck C T, Tewari S, Thoma J and Virosztek A 1995 *Phys. Rev.* B **51** 3797
[6] Mott N F 1990 *Metal–Insulator Transitions* 2nd edn (New York: Taylor and Francis) pp 123–44, 171–97
[7] Bao W, Broholm C, Carter S A, Rosenbaum T F and Aeppli G 1993 *Phys. Rev. Lett.* **71** 766
[8] Fawcett E 1988 *Rev. Mod. Phys.* **60** 209
[9] Herring C 1966 *Magnetism* vol 4, ed G T Rado and H Suhl (New York: Academic) pp 85–119
[10] Overhauser A W 1962 *Phys. Rev.* **128** 1437
[11] Noakes D R, Holden T M, Fawcett E and deCamargo P C 1990 *Phys. Rev. Lett.* **65** 369
[12] Hayden S M, Doubble R, Aeppli G, Perring T G, Fawcett E, Lowden J and Mitchell P W 1997 *Physica* B **237+238** 421
[13] Holden T M, Menshikov A Z and Fawcett E 1996 *J. Phys.: Condens. Matter* **8** L291
[14] Mason T E, Adams C P, Mentink S A M, Fawcett E, Menshikov A Z, Frost C D, Forsyth J B, Perring T G and Holden T M 1997 *Physica* B **237+238** 449
[15] Paul D M^{c}K, Mitchell P W, Mook H A and Steigenberger U 1988 *Phys. Rev.* B **38** 580
[16] Mook H A and Paul D M^{c}K 1985 *Phys. Rev. Lett.* **54** 227
[17] Vasiliu-Doloc L, Lynn J W, Moudden A H, de Leon-Guevara A M and Revcolevschi A 1998 *Phys. Rev.* B **58** 14 913
[18] Corliss L M, Hastings J M, Kunnmann W, Thomas R, Zhuang J, Butera R and Mukamel D 1985 *Phys. Rev.* B **31** 4337
[19] Menshikov A Z, Dorofeev Yu A, Budrina G L and Syromyatnikov V M 1988 *J. Magn. Magn. Mater.* **73** 211
[20] Lovesey S M 1984 *Theory of Inelastic Neutron Scattering* vol 2 (New York: Oxford University Press) pp 109–19
[21] Villain J 1973 *J. Phys. C: Solid State Phys.* **6** L97
[22] Brown P J 1995 *International Tables for Crystallography* vol C, ed A J C Wilson (Boston, MA: Kluwer Academic) p 392
[23] Cooke J F, Lynn J W and Davis H L 1980 *Phys. Rev.* B **21** 4118
[24] Halperin B I and Hohenberg P C 1969 *Phys. Rev.* **177** 952
[25] Fukuda T and Endoh Y 1998 *Physica* B **241–243** 619